crystals

MDPI

Communication

Designer Synthesis of Ultra-Fine Fe-LTL Zeolite Nanocrystals

Fen Zhang [1,*], Yunhong Luo [1], Lei Chen [2], Wei Chen [1], Yin Hu [1], Guihua Chen [1], Shengyong You [1] and Weiguo Song [1,3]

1 Institute of Applied Chemistry, Jiangxi Academy of Sciences, Nanchang 330096, China; 201814060201@stu.ncst.edu.cn (Y.L.); chenwei@jxas.ac.cn (W.C.); huyin@jxas.ac.cn (Y.H.); chenguihua@jxas.ac.cn (G.C.); youshengyong@jxas.ac.cn (S.Y.); wsong@iccas.ac.cn (W.S.)

2 College of Chemistry and Chemical Engineering, Jiangxi Normal University, Nanchang 330022, China; chenlei1999@jxnu.edu.cn

3 Institute of Chemistry, Chinese Academy of Sciences, Beijing 100190, China

* Correspondence: zhangfen@jxas.ac.cn

Received: 28 August 2020; Accepted: 14 September 2020; Published: 15 September 2020



Abstract: Nanosized zeolites with larger external surface area and decreased diffusion pathway provide many potential opportunities in adsorption, diffusion, and catalytic applications. Herein, we report a designer synthesis of ultra-fine Fe-LTL zeolite nanocrystals under very mild synthesis conditions. We prepared Fe-LTL zeolite nanocrystals synthesized using L precursor. The precursor is aging at room temperature to obtain zeolite L nuclei. In order to investigate more details of Fe-LTL zeolite nanocrystals, various characterizations including X-ray diffraction (XRD), inductively coupled plasma (ICP), diffuse reflectance ultraviolet-visible (UV-Vis) spectroscopy, confirm the tetrahedral Fe^{3+} species in the zeolite framework. Besides, scanning electron microscope (SEM), Fourier transform infrared spectrometer (FT-IR), dynamic light scattering (DLS) indicate that the average particle size of Fe-LTL zeolite crystals is approximately 30 nm. Thus, ultra-fine Fe-LTL zeolite with large external surface area and shorter diffusion pathway to the active sites might have great potential in the near future.

Keywords: zeolite L precursor; Fe-LTL zeolite; ultra-fine

1. Introduction

Zeolites as promising adsorbents, ion-exchangers, and catalysts have been widely used in the fields of catalysis, separations, and adsorption [1–14]. In particular, they have accelerated the development of heterogeneous catalysis and separation processes because of their large internal surface area, unique channel systems, high pore volume, and adjustable active sites. The chemical composition and pore architecture of zeolites are important, however, the precise control of their crystallite morphology also has a significant influence on their applications in catalysis and adsorption. As the crystal size decreases below 100 nm, the zeolite external surface area, which is distinct from the internal pore surface and is negligible for micron-sized zeolites, increases dramatically, resulting in zeolites with over 25% of the total surface area on the external surface [15]. Shorter diffusion path length of nanosized zeolites is another advantage compared to micron-sized zeolites. The improved properties of nanosized zeolites for adsorption and diffusion provide many potential opportunities for their applications in environmental catalysis, environmental remediation, decontamination, and drug delivery [16]. Thus, zeolite nanocrystals have been paid much attention because of their widespread applications, the strategies for the preparation of zeolite nanocrystals are necessary and important [17–21]. Nonetheless, designer synthesis of pure zeolite nanocrystals is still challenging at present.

The structure of zeolite LTL is hexagonal (space group P6/mmm) with unit cell constants a = 18.4 Å and c = 7.5 Å [22]. The linkages of the cancrinite cages by double 6-rings (D6R) lead to the formation of columns in the c-direction and thus give rise to 12-membered rings with a free diameter of 7.1 Å [23]. Over past 20 years, zeolite L has drawn much attention for their applications in catalytic processes [24–27], ion-exchange and separations [28,29], and photonic devices [30,31]. Notably, iron catalysts, supported on different solids, have been widely applied in Fischer-Tropsch reaction for many years. Combining the advantages of iron and LTL zeolites, it is very meaningful to synthesize ultra-fine Fe-LTL zeolite nanocrystals, which are potentially significant for catalytic applications.

Herein, we report a designer synthesis of ultra-fine Fe-LTL zeolite nanocrystals under very mild synthesis conditions. We prepared Fe-LTL zeolite nanocrystals synthesized using L precursor. The precursor is aging at room temperature to obtain zeolite L nuclei. Notably, the average crystal size of Fe-LTL zeolite nanocrystals we obtained is approximately 30 nm, which is smaller than the previous reports. In order to investigate more details of Fe-LTL zeolite nanocrystals, various characterizations including X-ray diffraction (XRD), diffuse reflectance ultraviolet-visible (UV-Vis) spectroscopy, confirm the tetrahedral Fe^{3+} species in the zeolite framework. Besides, scanning electron microscope (SEM), Fourier transform infrared spectrometer (FT-IR), dynamic light scattering (DLS) indicate the nanoscale of zeolite crystals. Ultra-fine Fe-LTL zeolite with large external surface area and shorter diffusion pathway to the active sites might have great potential in the near future.

2. Materials and Methods

2.1. Materials

The following chemicals were utilized: sodium aluminate ($NaAlO_2$, 36.6% Na_2O, and 43.3% Al_2O_3, Sinopharm Chemical Reagent Co., Ltd., Shanghai, China), sodium hydroxide (NaOH, AR, 96%, Sinopharm Chemical Reagent Co., Ltd., Shanghai, China), potassium hydroxide (KOH, AR, 85%, Sinopharm Chemical Reagent Co., Ltd., Shanghai, China), silica sol (LUDOX HS-40, 40% SiO_2 in water, Sigma Aldrich, St. Louis, MO, USA), aluminum sulfate ($Al_2(SO_4)_3{\cdot}18H_2O$, AR, 99%, Sinopharm Chemical Reagent Co., Ltd., Shanghai, China), sodium silicate solution (253.8 g/L SiO_2, 77.8 g/L Na_2O of 1 L sodium silicate solution), ferric chloride hexahydrate ($FeCl_3{\cdot}6H_2O$, AR, Sinopharm Chemical Reagent Co., Ltd., Shanghai, China)

2.1.1. Synthesis of Zeolite L Precursor

As a typical run, zeolite L precursor was prepared by mixing 10 mL deionized H_2O, 0.472 g sodium aluminate and 3.76 g potassium hydroxide under stirring for 10 min, 8.4 g silica sol was added later. After the solution was stirred for 1 h, 0.24 g sodium hydroxide was finally added, followed by aging at room temperature for 72 h, giving a clear solution. The molar ratio of the precursor is $3.0Na_2O/14.3K_2O/Al_2O_3/28SiO_2/413H_2O$.

2.1.2. Synthesis of Fe-L Samples

Zeolite Fe-L nanocrystals were hydrothermally synthesized at the temperature of 80 °C for 3 days with $2.1Na_2O/3.4K_2O/Al_2O_3/15SiO_2/0.6FeCl_3/250H_2O$ molar ratios of initial synthesis gels in the presence of zeolite L precursor. As a typical run, 1.16 g potassium hydroxide was added to 10.9 g sodium silicate solution, followed by introducing 1.4 g deionized H_2O. After stirring for about 1 h, 1.665 g aluminum sulfate was added to the mixture, followed by the addition of 0.4 g $FeCl_3{\cdot}6H_2O$, finally the last addition of 2.0 mL zeolite L precursor. After being stirred for 2 h at room temperature, the mixture was transferred into an autoclave to crystallize at 80 °C for 3 days. The products were collected by filtration, washed with deionized H_2O, and dried in air, respectively. The H-form of the samples was prepared by triple ion-exchange with 1M of NH_4NO_3 solution at 80 °C for 1 h and calcination at 550 °C for 5 h.

2.1.3. Synthesis of Conventional Fe-L Zeolite

Conventional Fe-L crystal was hydrothermally synthesized at the temperature of 180 °C for 1 day with $1.56K_2O/Al/6.25SiO_2/0.25FeCl_3/90H_2O$ molar ratios of starting gels. The product was collected by filtration, washed with deionized H_2O, and dried in air. The H-form of the sample was prepared by triple ion-exchange with 1M of NH_4NO_3 solution at 80 °C for 1 h and calcination at 550 °C for 5 h.

2.2. Methods

Powder X-ray diffraction (XRD) (Rigaku, Tokoyo, Japan) data were experimented at room temperature with a Rigaku Ultimate VI X-ray diffractometer (40 kV, 40 mA) using CuKα (λ = 1.5406 Å) radiation. Crystallinity of samples is calculated by area of peaks at 5.7°, 19°, 22°, and 28° from the XRD patterns. Scanning electron microscopy (SEM) (Hitachi, Tokoyo, Japan) experiments were carried out on Hitachi SU-8010 and SU-1510 electron microscopes. Dynamic light scattering (DLS) (Malvern, Malvern City, UK) experiments were measured using a Malvern Instrument Zetasizer Nano ZS90. Nitrogen sorption experiments (Micromeritics, Atlanta, GA, USA) were performed on a Micromeritics TriStar II at −196 °C. The pore volume and surface area were calculated using the t-plot and BET methods. UV-Vis analysis, using $BaSO_4$ as the internal standard sample was performed on a Perkin-Elmer Lambda 20 spectrometer (Perkin Elmer, Waltham, MA, USA). Fourier transform infrared spectrometer (FT-IR) was measured on a FTIR 7600 Spectrometer (Lambda, Sydney, Australia). The sample composition was tested by ICP with a Perkin-Elmer 3300DV emission spectrometer.

3. Results and Discussion

Figure 1a–d shows the XRD patterns of as-synthesized and calcined Fe-LTL nanocrystals (Fe-LTL-N), conventional Fe-LTL (Fe-LTL-C), and calcined Fe-LTL-N, Fe-LTL-C samples. These samples give a series of characteristic peaks of the LTL framework structure. The peaks of Fe-LTL-N are broader than those of Fe-LTL-C, indicating the crystal size of Fe-LTL-N samples is nanoscale. After calcination, these peaks are basically remained, indicating their good thermal stability.

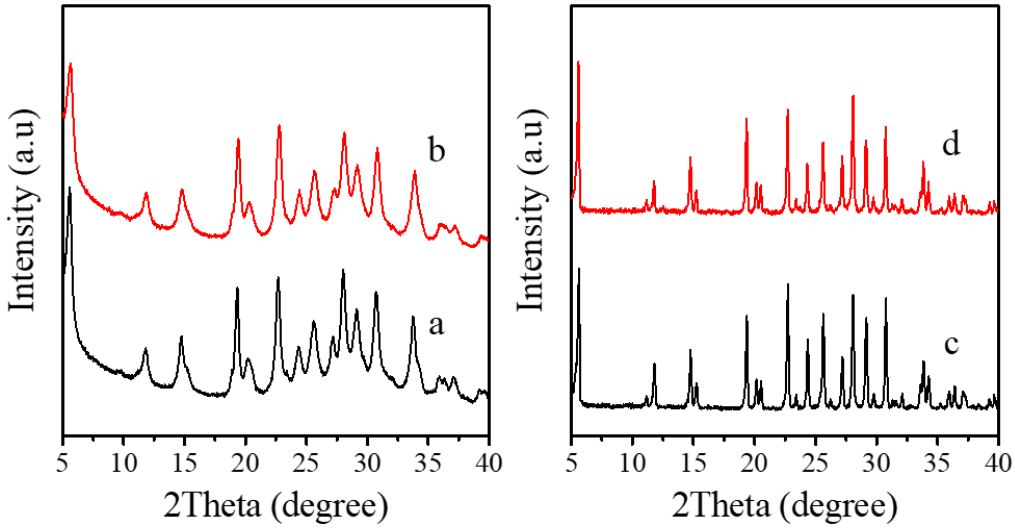


Figure 1. XRD patterns of (**a**) as-synthesized Fe-LTL-N, (**b**) calcined Fe-LTL-N, (**c**) as-synthesized Fe-LTL-C, (**d**) calcined Fe-LTL-C, respectively.

Figure 2 gives the SEM images of as-synthesized Fe-LTL-N, Fe-LTL-C samples. Figure 2a exhibits nanocylindrical morphology of Fe-LTL-N with size of 20–50 nm, while the morphology of Fe-LTL-C is micron cylindrical (Figure 2b). It is well consistent with the result from XRD testing of Fe-LTL-N and Fe-LTL-C samples. The particle size distribution (Figure 3) shows the average particle size of Fe-LTL-N is 30 nm. Notably, agglomeration of Fe-LTL-N is also exhibited in Figure 2a. Zeolite nanocrystals with

smaller sizes have higher relative surface area and higher energy. To minimize its surface energy the nanocrystals create agglomeration.

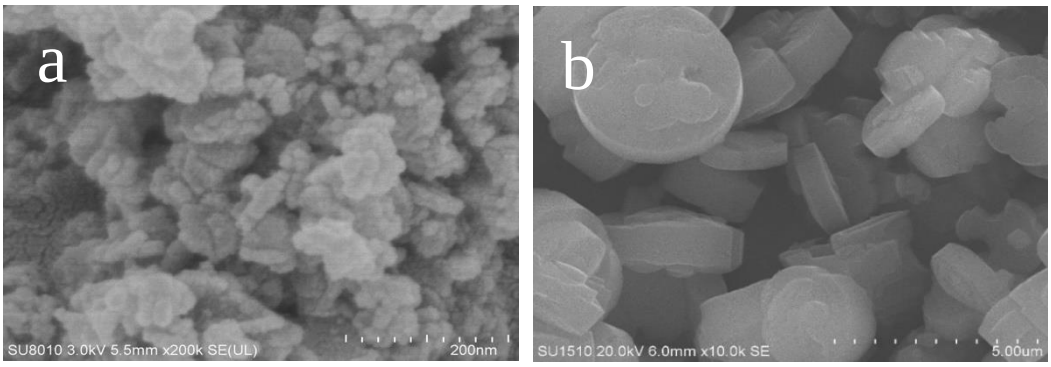


Figure 2. SEM images of as-synthesized (**a**) Fe-LTL-N, (**b**) Fe-LTL-C.

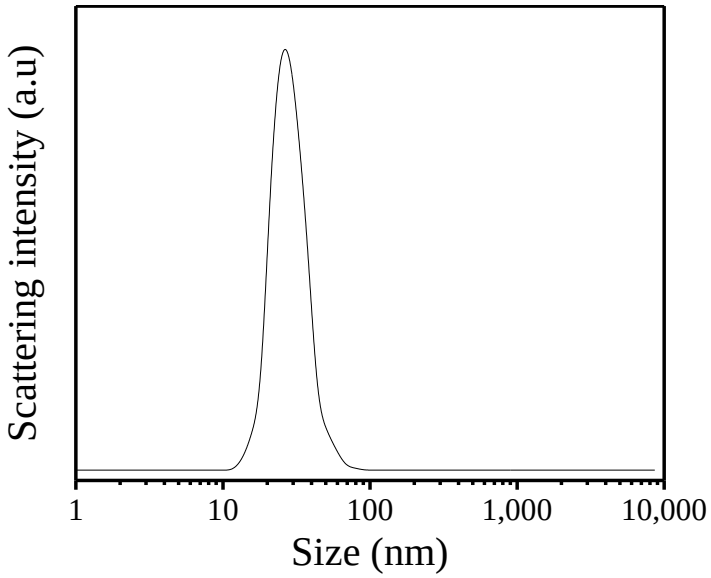


Figure 3. DLS curve of as-synthesized Fe-LTL-N.

The porosity and specific surface area of Fe-LTL-N and Fe-LTL-C samples were characterized by nitrogen adsorption measurement (Figure 4a,b), which displays the related parameters, as shown in Table 1. Fe-LTL-N sample shows a mixed isotherm curve of Type I and IV with a large H1-type hysteresis. As the Table 1 shows, the total pore volume of Fe-LTL-N is 0.38 cm^3g^{-1}, while the conventional Fe-LTL zeolite shows relatively low pore volume at only 0.19 cm^3g^{-1}. The results are consistent with that of XRD patterns and SEM images.

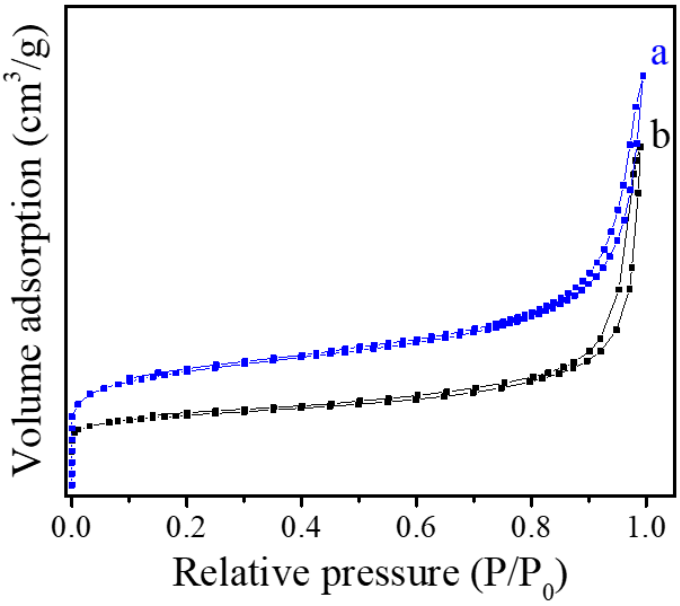


Figure 4. N_2 isotherm sorption of (**a**) Fe-LTL-N, (**b**) Fe-LTL-C.

Table 1. Textural parameters of Fe-LTL samples.

Sample	S_{BET} (m^2g^{-1})	S_{micro} (m^2g^{-1})	V_{total} (cm^3g^{-1})	V_{micro} (cm^3g^{-1})
Fe-LTL-N	285	228	0.38	0.10
Fe-LTL-C	142	128	0.19	0.12

Figure 5 displays the UV-vis spectrum of Fe-LTL-N, exhibiting a strong absorption band at 220 nm with a distinct shoulder at 245 nm and weak bands at 379, 419, and 446 nm, which is in good agreement with the previously reported results [32]. Both bands in the 220–250 nm range correspond to tetrahedral Fe in the zeolite, where the band at 220 nm may be due to a different specific environment of Fe within the zeolite framework. The absorption bands located at 379, 419, and 446 nm are assigned to tetrahedral Fe^{3+} in the zeolite framework [33]. There were no obvious absorption peaks at near 320 nm, indicating the absence of aggregated FeO_x species in the extra-framework.

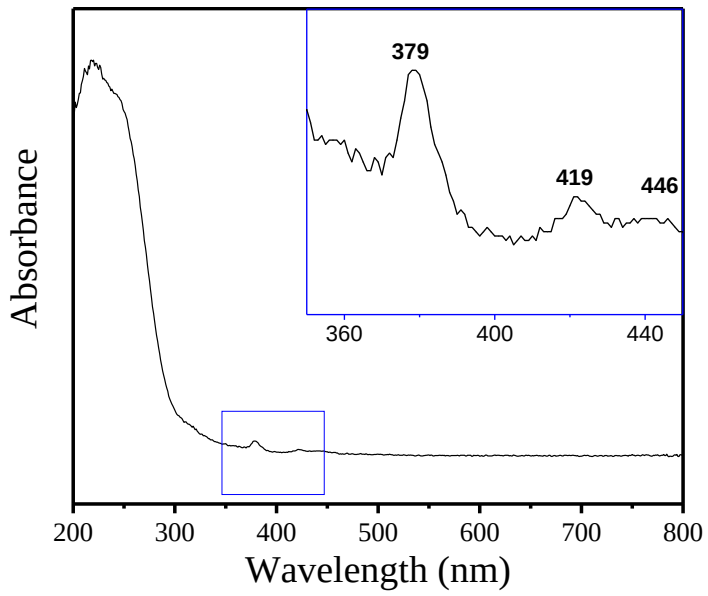


Figure 5. UV-vis spectrum of as-synthesized Fe-LTL-N.

Table 2 presents a systematic investigation on crystallization of Fe-LTL zeolite nanocrystals at 80 °C from aluminosilicate gels in the presence of L precursor. Interestingly, when the K_2O/SiO_2 in the gels is optimized from 0.122 to 0.300, products of amorphous phase are obtained such as, a mixture of amorphous phase with LTL structure, pure LTL, a mixture of LTL and amorphous (Figure 6A). However, as the K_2O/SiO_2 ratio in the synthesis gel increases, there is significant broadening and a decrease in height for peaks. Notably, sample obtained under Run 6 with poorer crystallinity shows decrease in height of resolved IR spectrum compared with Fe-LTL-N sample (Figure S1). Combined with the XRD pattern of sample (Run 6), it is probably a mixture of LTL and amorphous [34]. Moreover, the suitable K_2O/SiO_2 ratio for crystallization of pure LTL structure is changed from 0.229 to 0.265. It is found that the SiO_2/Al_2O_3 ratio has a great influence on the crystallization of LTL zeolite. When the SiO_2/Al_2O_3 ratio is less than 15, it is normally amorphous phase. When this ratio is distributed in the range of 15–25, a pure phase of LTL structure is usually formed (Figure 6B). Figure S1 also shows resolved IR spectra of samples obtained under conditions of Run 10 and 11. Obviously, sample (Run 10) gives similar IR spectrum as that of sample (Run 6), while sample (Run 11) has a further decrease in height for the peaks. Therefore, the sample synthesized under Run 10 and 11 are probably mixture of LTL and amorphous. Furthermore, the $FeCl_3/SiO_2$ ratio also influences the crystallization of Fe-LTL zeolite. The Fe content and Si/Al ratios of samples is listed in Table 3. Clearly, samples obtained with more iron content in the initial gel are likely to exhibit higher iron content and Si/Al ratios. As the Figure 6C shows, the increase of iron content up to a certain amount in the initial synthesis gels tends to produce samples with lower crystallinity. When this ratio in the initial gel reaches to 0.07, it is formed a mixture of LTL with amorphous. It has been claimed that the presence of greater concentrations of iron in the gel inhibited the formation of the cancrinite cage due to the larger Fe-O bond length compared to Al-O [34]. Moreover, cancrinite cage is crucial in the formation of LTL zeolites. Thus, the amount of iron in the synthesis gels really has a major impact on crystallinity of Fe-LTL zeolites. Moreover, crystallization temperature has a great effect on the crystallization of zeolite crystals. Figure 7 shows the XRD patterns of Fe-LTL zeolite nanocrystals synthesized with the same ratios of Run 4 at different crystallization temperatures. Reasonably, higher crystallization of Fe-LTL zeolites tends to be obtained at higher crystallization temperatures.

Table 2. Impact of synthesis conditions on crystallization of Fe-LTL zeolite nanocrystals (Na_2O/SiO_2 = 0.14, H_2O/SiO_2 = 250, at 80 °C for 3 d).

Run	K_2O/SiO_2	SiO_2/Al_2O_3	$FeCl_3/SiO_2$	Product [a]	Crystallinity [b] (%)	Yield [c] (%)
1	0.122	15	0.04	Amor	/	/
2	0.158	15	0.04	Amor	/	/
3	0.193	15	0.04	Amor+LTL	/	/
4	0.229	15	0.04	LTL	100	40
5	0.265	15	0.04	LTL	65	56
6	0.300	15	0.04	LTL + Amor	/	/
7	0.229	10	0.04	Amor	/	/
8	0.229	20	0.04	LTL	65	36
9	0.229	25	0.04	LTL	80	30
10	0.229	30	0.04	LTL + Amor	/	/
11	0.229	40	0.04	LTL + Amor	/	/
12	0.229	15	0.03	LTL	100	30
13	0.229	15	0.05	LTL	100	67
14	0.229	15	0.06	LTL	100	72
15	0.229	15	0.07	LTL + Amor	/	/
16	0.229	15	0.08	LTL + Amor	/	/

[a] The phase appearing first is dominant. [b] Run 4 was designated as 100% crystallinity. [c] yield (%) = quantity of product*100/quantity of SiO_2 in the synthesis gel.

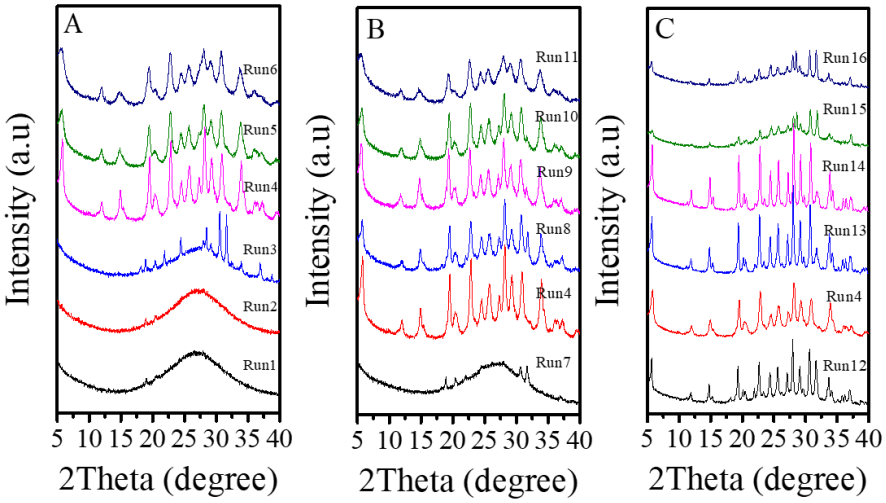


Figure 6. XRD patterns of Fe-LTL zeolite crystals synthesized under various conditions in Table 2. (**A**) XRD patterns of Fe-LTL zeolite crystals synthesized with different K_2O/SiO_2 ratios; (**B**) XRD patterns of Fe-LTL zeolite crystals synthesized with different SiO_2/Al_2O_3 ratios; (**C**) XRD patterns of Fe-LTL zeolite crystals synthesized with different $FeCl_3/SiO_2$ ratios.

Table 3. Fe/Si and Si/Al ratios of different samples.

Run	Fe/Si Ratio in the Initial Gel	Fe Content in the Obtained Sample [d]	Si/Al Ratio in the Obtained Sample [d]
12	0.03	2.07%	4.6
4	0.04	2.67%	4.7
13	0.05	3.33%	4.6
14	0.06	3.10%	5.3
15	0.07	3.74%	5.8
16	0.08	3.34%	5.9

[d] The iron content and Si/Al ratio was tested by ICP experiment.

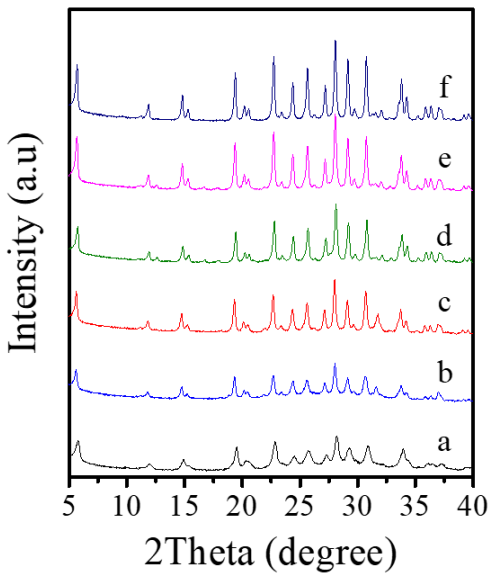


Figure 7. XRD patterns of Fe-LTL zeolite crystals synthesized at (**a**) 80 °C, (**b**) 100 °C, (**c**) 120 °C, (**d**) 140 °C, (**e**) 160 °C, (**f**) 180 °C, respectively.

After the systematic synthesis, aluminosilicate gel for crystallization of Fe-LTL zeolites at 80 °C with molar ratio of $2.1Na_2O/3.4K_2O/Al_2O_3/15SiO_2/0.6FeCl_3/250H_2O$ is suitable.

4. Conclusions

In summary, we have successfully synthesized ultra-fine Fe-LTL zeolite nanocrystals under very mild synthesis conditions. The average particle size of Fe-LTL zeolite nanocrystals is approximately 30 nm. Moreover, Fe-LTL-N zeolites that we obtained have advantages of larger external surface area, shorter diffusion pathway, good thermal stability, narrow particle distribution. Very importantly, tetrahedral Fe^{3+} is located in the zeolite framework of Fe-LTL-N. Designer synthesis of ultra-fine Fe-LTL zeolite nanocrystals in this work has significant potential applications for industrial catalysis in the near future.

Supplementary Materials: The following are available online at http://www.mdpi.com/2073-4352/10/9/813/s1, Figure S1: IR spectra of Fe-LTL zeolite crystals synthesized under various conditions in Table 2.

Author Contributions: Conceptualization and writing, F.Z.; methodology, Y.L., L.C. and G.C.; investigation, W.C., Y.H., S.Y., and W.S. All authors have read and agreed to the published version of the manuscript.

Funding: This research was funded by the Jiangxi Provincial Natural Science Foundation (20202ACB203003), the Science and Technology Program of Jiangxi Academy of Sciences (2020-YZD-3, 2019-XTPH1-09, 2019-YYB-09, 2018-YDHZ-01).

Conflicts of Interest: The authors declare no conflict of interest.

References

1. Davis, M.E.; Lobo, R.F. Zeolite and molecular sieve synthesis. Chemistry of Materials. *Chem. Mater.* **1992**, *4*, 756–768. [CrossRef]
2. Gies, H.; Marler, B. The structure-controlling role of organic templates for the synthesis of porosils in the system SiO_2/template/H_2O. *Zeolite* **1992**, *12*, 42–49. [CrossRef]
3. Davis, M.E. Ordered porous materials for emerging applications. *Nature* **2002**, *417*, 813–821. [CrossRef]
4. Cundy, C.S.; Cox, P.A. The hydrothermal synthesis of zeolites: History and development from the earliest days to the present time. *Chem. Rev.* **2003**, *103*, 663–702. [CrossRef] [PubMed]
5. Zou, X.; Conradsson, T.; Klingstedt, M.; Dadachov, M.S.; O'Keeffe, M. A mesoporous germanium oxide with crystalline pore walls and its chiral derivative. *Nature* **2005**, *437*, 716–719. [CrossRef] [PubMed]
6. Ma, S.Q.; Sun, D.F.; Wang, X.S.; Zhou, H.C. A mesh-adjustable molecular sieve for general use in gas separation. *Angew. Chem. Int. Ed.* **2007**, *46*, 2458–2462. [CrossRef] [PubMed]
7. Shin, J.; Camblor, M.A.; Woo, H.C.; Miller, S.R.; Wright, P.A.; Hong, S.B. PST-1: A synthetic small-pore zeolite that selectively adsorbs H_2. *Angew. Chem. Int. Ed.* **2009**, *48*, 6647–6650. [CrossRef] [PubMed]
8. Lee, J.H.; Park, M.B.; Lee, J.K.; Min, H.K.; Song, M.K.; Hong, S.B. Synthesis and characterization of ERI-type UZM-12 zeolites and their methanol-to-olefin performance. *J. Am. Chem. Soc.* **2010**, *132*, 12971–12982. [CrossRef]
9. Na, K.; Jo, C.; Kim, J.; Cho, K.; Jung, J.; Seo, Y.; Messinger, R.J.; Chmelka, B.F.; Ryoo, R. Directing zeolite structures into hierarchically nanoporous architectures. *Science* **2011**, *333*, 328–332. [CrossRef] [PubMed]
10. Zhang, X.Y.; Liu, D.X.; Xu, D.D.; Asahina, S.; Cychosz, K.A.; Agrawal, K.V.; Al Wahedi, Y.; Bhan, A.; Al Hashimi, S.; Terasaki, O.; et al. Synthesis of self-pillared zeolite nanosheets by repetitive branching. *Science* **2012**, *336*, 1684–1687. [CrossRef]
11. Goel, S.; Wu, Z.J.; Zones, S.I.; Iglesia, E. Synthesis and catalytic properties of metal clusters encapsulated within small-pore (SOD, GIS, ANA) zeolites. *J. Am. Chem. Soc.* **2012**, *134*, 17688–17695. [CrossRef]
12. Jo, C.; Jung, J.; Shin, H.S.; Kim, J.; Ryoo, R. Capping with Multivalent Surfactants for Zeolite Nanocrystal Synthesis. *Angew. Chem. Int. Ed.* **2013**, *52*, 10014–10017. [CrossRef]
13. Moller, K.; Bein, T. Mesoporosity-a new dimension for zeolites. *Chem. Soc. Rev.* **2013**, *42*, 3689–3707. [CrossRef] [PubMed]
14. Bian, C.Q.; Wang, X.; Yu, L.; Zhang, F.; Zhang, J.; Fei, Z.X.; Qiu, J.P.; Zhu, L.F. Generalized methodology for inserting metal heteroatoms into the layered zeolite precursor RUB-36 by interlayer expansion. *Crystals* **2020**, *10*, 530. [CrossRef]
15. Song, W.; Justice, R.E.; Jones, C.A.; Grassian, V.H.; Larsen, S.C. Size-dependent properties of nanocrystalline silicalite synthesized with systematically varied crystal sizes. *Langmuir* **2004**, *20*, 4696–4702. [CrossRef] [PubMed]

16. Larsen, S.C. Nanocrystalline zeolites and zeolite structures: Synthesis, characterization, and applications. *J. Phys. Chem. C* **2007**, *111*, 18464–18474. [CrossRef]
17. Choi, M.; Na, K.; Kim, J.; Sakamoto, Y.; Terasaki, O.; Ryoo, R. Stable single-unit-cell nanosheets of zeolite MFI as active and long-lived catalysts. *Nature* **2009**, *461*, 246–249. [CrossRef]
18. Eng-Poh, N.; Chateigner, D.; Bein, T.; Valtchev, V.; Mintova, S. Capturing ultrasmall EMT zeolite from template-free systems. *Science* **2012**, *335*, 70–73.
19. Feng, G.D.; Cheng, P.; Yan, W.F.; Boronat, M.; Li, X.; Su, J.H.; Wang, J.Y.; Li, Y.; Corma, A.; Xu, R.R. Accelerated crystallization of zeolites via hydroxyl free radicals. *Science* **2016**, *351*, 1188–1191. [CrossRef]
20. Chen, W.; Fan, Z.L.; Pan, X.L.; Bao, X.H. Effect of confinement in carbon nanotubes on the activity of Fischer-Tropsch iron catalyst. *J. Am. Chem. Soc.* **2008**, *130*, 9414–9419. [CrossRef]
21. Awala, H.; Gilson, J.-P.; Retoux, R.; Boullay, P.; Goupil, J.-M.; Valtchev, V.; Mintova, S. Template-free nanosized faujasite-type zeolites. *Nat. Mater.* **2015**, *14*, 447–451. [CrossRef] [PubMed]
22. Ohsuna, T.; Horikawa, Y.; Hiraga, K.; Terasaki, O. Surface Structure of Zeolite L Studied by High-Resolution Electron Microscopy. *Chem. Mater.* **1998**, *10*, 688–691. [CrossRef]
23. Laulus, O.; Valtchev, V.P. Crystal morphology control of LTL-type zeolite crystals. *Chem. Mater.* **2004**, *16*, 3381–3389.
24. Davis, R.J. Aromatization on zeolite L-supported Pt clusters. *Heterogen. Chem. Rev.* **1994**, *1*, 41–53.
25. Joshi, P.N.; Bandyopadhyay, R.; Awate, S.V.; Shiralkar, V.P.; Rao, B.S. Influence of physicochemical parameters on n-hexane dehydrocyclization over Pt/LTL zeolites. *React. Kinet. Catal. Lett.* **1994**, *53*, 231–236. [CrossRef]
26. Jentoft, R.E.; Tsapatsis, M.; Davis, M.E.; Gates, B.C. Platinum clusters supported in zeolite LTL: Influence of catalyst morphology on performance in n-hexane reforming. *J. Catal.* **1998**, *179*, 565–580. [CrossRef]
27. Miller, J.T.; Agrawal, N.G.B.; Lane, G.S.; Modica, F.S. Effect of pore geometry on ring closure selectivities in platinum L-zeolite dehydrocyclization catalysts. *J. Catal.* **1996**, *163*, 106–116. [CrossRef]
28. Barrer, R.M.; Galabova, I.M. Ion-exchanged forms of zeolite L, erionite, and offretite and sorption of inert-gases. *Adv. Chem. Ser.* **1973**, 356–373. [CrossRef]
29. Lee, T.P.; Saad, B.; Ng, E.P.; Salleh, B. Zeolite linde type L as micro-solid phase extraction sorbent for the high performance liquid chromatography determination of ochratoxin A in coffee and cereal. *J. Chromatogr. A* **2012**, *1237*, 46–54. [CrossRef]
30. Calzaferri, G.; Huber, S.; Maas, H.; Minkowski, C. Host–Guest Antenna Materials. *Angew. Chem. Int. Ed.* **2003**, *42*, 3732–3735. [CrossRef]
31. Gigli, L.; Arletti, R.; Tabacchi, G.; Fabbiani, M.; Vitillo, J.G.; Martra, G.; Devaux, A.; Miletto, I.; Quartieri, S.; Calzaferri, G. Structure and host-guest interactions of perylene-diimide dyes in zeolite L nanochannels. *J. Phys. Chem. C.* **2018**, *122*, 3401–3418. [CrossRef]
32. Goldfarb, D.; Bernado, M.; Strohmaier, K.G.; Vaughan, D.E.W.; Thomann, H. Characterization of iron in zeolites by X-band and Q-band ESR, pulsed ESR, and UV-visible spectroscopies. *J. Am. Chem. Soc.* **1994**, *116*, 6344–6353. [CrossRef]
33. Zhang, H.; Chu, L.; Xiao, Q.; Zhu, L.; Yang, C.; Meng, X.; Xiao, F.-S. One-pot synthesis of Fe-Beta zeolite by an organotemplate-free and seed-directed route. *J. Mater. Chem. A* **2013**, *1*, 3254–3257. [CrossRef]
34. Camblor, M.A.; Corma, A.; Mifsud, A.; Perez-Pariente, J. Valencia, Synthesis of nanocrystalline zeolite Beta in the absence of alkali metal cations. *Stud. Surf. Sci. Catal.* **1997**, *105*, 341–348.



© 2020 by the authors. Licensee MDPI, Basel, Switzerland. This article is an open access article distributed under the terms and conditions of the Creative Commons Attribution (CC BY) license (http://creativecommons.org/licenses/by/4.0/).